inorganics

MDPI

Article

The *Trans* Influence in Unsymmetrical Pincer Palladacycles: An Experimental and Computational Study

Sarote Boonseng [1], Gavin W. Roffe [1], Rhiannon N. Jones [1], Graham J. Tizzard [2], Simon J. Coles [2], John Spencer [1,*] and Hazel Cox [1,*]

[1] Department of Chemistry, School of Life Sciences, University of Sussex, Falmer, Brighton, East Sussex, BN1 9QJ, UK; s.boonseng@sussex.ac.uk (S.B.); gwr20@sussex.ac.uk (G.W.R.); R.N.Jones@sussex.ac.uk (R.N.J.)

[2] UK National Crystallography Service, School of Chemistry, University of Southampton, Highfield, Southampton, SO17 1BJ, UK; Graham.Tizzard@soton.ac.uk (G.J.T.); S.J.Coles@soton.ac.uk (S.J.C.)

* Correspondence: j.spencer@sussex.ac.uk (J.S.); h.cox@sussex.ac.uk (H.C.); Tel.: +44-1273-877-374 (J.S.); +44-1273-678-972 (H.C.)

Academic Editor: Duncan H. Gregory
Received: 24 June 2016; Accepted: 5 August 2016; Published: date

Abstract: A library of unsymmetrical SCN pincer palladacycles, [ClPd{2-pyr-6-(RSCH$_2$)C$_6$H$_3$}], R = Et, Pr, Ph, *p*-MePh, and *p*-MeOPh, pyr = pyridine, has been synthesized via C–H bond activation, and used, along with PCN and N'CN unsymmetrical pincer palladacycles previously synthesized by the authors, to determine the extent to which the *trans* influence is exhibited in unsymmetrical pincer palladacycles. The *trans* influence is quantified by analysis of structural changes in the X-ray crystal and density functional theory (DFT) optimized structures and a topological analysis of the electron density using quantum theory of atoms in molecules (QTAIM) to determine the strength of the Pd-donor atom interaction. It is found that the *trans* influence is controlled by the nature of the donor atom and although the substituents on the donor-ligand affect the Pd-donor atom interaction through the varied electronic and steric constraints, they do not influence the bonding of the ligand *trans* to it. The data indicate that the strength of the *trans* influence is P > S > N. Furthermore, the synthetic route to the family of SCN pincer palladacycles presented demonstrates the potential of late stage derivitization for the effective synthesis of ligands towards unsymmetrical pincer palladacycles.

Keywords: pincer palladacycles; density functional theory; atoms in molecules; *trans* influence

1. Introduction

Palladacycles have been extensively studied since their discovery in 1965 by Cope and Siekman [1]. They have been widely used as catalysts or pre-catalysts in organic reactions, such as in Heck and Suzuki–Miyaura cross-couplings [2–5]. Pincer palladacycles are an interesting type of palladacycle, of which there are two different types. The majority of pincer palladacycles studied have been of the symmetrical YCY type, such as NCN [6], SCS [7], PCP [8], and SeCSe [9,10]. There are limited numbers of reported unsymmetrical pincer palladacycles owing to their more difficult synthesis. For example, Szabó et al. synthesized unsymmetrical PCS pincer palladacycles from 1,3-bis(bromomethyl)benzene, albeit in low overall yield (38%) [11]. However, the unsymmetrical PCS pincer palladacycle reported showed enhanced catalytic activity when compared to related symmetrical pincer palladacycles [11,12]. Recently, we reported the synthesis of an unsymmetrical SCN pincer palladacycle by C–H bond activation [13], and novel unsymmetrical PCN and N'CN analogues [14] (Figure 1).

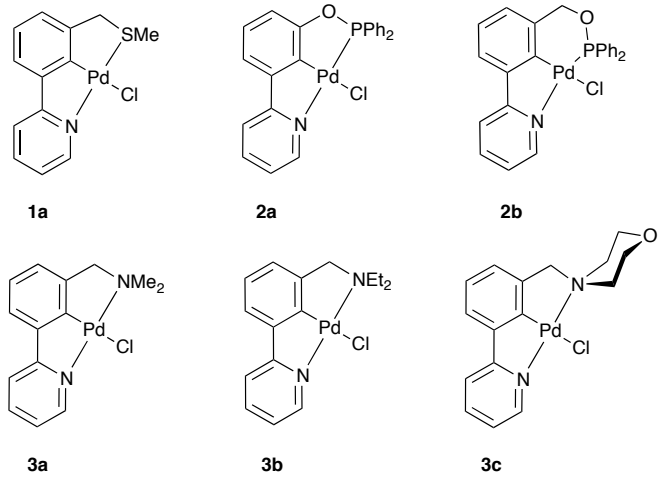

Figure 1. Unsymmetrical pincer palladacylces, SCN (**1a**) [13], PCN (**2a**–**2b**), and N′CN (**3a**–**3c**) [14].

The pincer palladacycle structures are stabilized by an intramolecular coordination to the metal of the two donor atoms in the side arms. Their reactivity and other properties are influenced by the donor group around the metal [3]. The attractive feature of pincer palladacycles is the possibility for fine-tuning the catalytic activity by varying the two side arms to modify the palladium environment, by changing the donor atoms and their substituents, providing the opportunity to alter hard/soft acid base properties, or by changing the ring size, giving rise to varying steric hindrance [12]. These factors provide the potential for hemilabile coordination of the donor ligand arms with the metal center, an important consideration in the design of pincer palladacycles [15–17]. This can lead to different physical and chemical properties of the donor ligand arms, resulting in preferential decoordination of one of the ligand arms, providing the opportunity to fine tune the catalytic activity of unsymmetrical pincer palladacycles [18–21]. An excellent example by Wendt and co-workers reported the hemilabile nature of nitrogen and phosphorus donor atoms by reacting with a strong nucleophile (MeLi) [22]. The results showed that the nitrogen donor atom arm decoordinated from the Pd center, while the phosphorus donor atom arm remained coordinated to the Pd center (Scheme 1). It is clear that the different properties of the side arms result in hemilability due to the changing strength and/or nature of interaction between donor atoms and the Pd center.

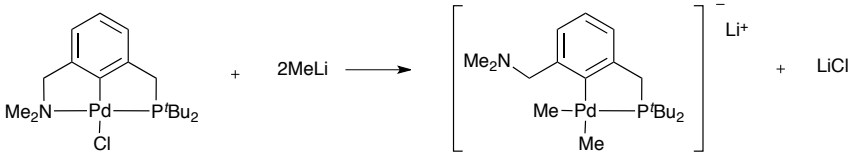

Scheme 1. Reaction of unsymmetrical pincer palladacycles with MeLi showing the hemilability of the nitrogen donor atom arm by Wendt et al. [22].

Pincer palladacycles exist in a square planar configuration at the Pd(II) center, and a key factor determining the strength of the interaction between Pd and the donor atoms is the *trans* influence, potentially affecting hemilability of donor atom arms. The *trans* influence is defined by Pidcock [23] as "the tendency of a ligand to weaken the bond *trans* to itself". The "*trans* influence" affects the structure in the ground, or thermodynamic state. Therefore, sometimes, it is called the thermodynamic *trans* effect, while the "*trans* effect" is related to the kinetic rate of reaction, depending on substitution of the bond *trans* to itself. The *trans* influence has been used to explain the stability of square planar complexes [24], while the *trans* effect has been used to study reaction pathways [25]. There are many experimental studies into the *trans* influence, generally using spectroscopic or X-ray crystallographic methods [26–28]. Additionally, density functional theory

(DFT) structure optimization and molecular orbital analysis have been employed in the study of the *trans* influence and give a good explanation of the *trans* influence in organometallic complexes [29–33].

In this study, we have investigated the *trans* influence in both model and experimentally-characterized unsymmetrical pincer palladacycles, using DFT calculations and quantum theory of atoms in molecules (QTAIM) analysis. Additionally, in order to determine the effect of varying the substituents on the donor atom, we have synthesized a library of unsymmetrical SCN pincer palladacycles, providing the opportunity to vary the steric and electronic properties on the sulfur atom. We have then used these palladacycles to further investigate the *trans* influence using DFT.

2. Results and Discussion

2.1. SCN Pincer Palladacycle Synthesis

Our previous work has demonstrated a novel synthetic route to an unsymmetrical SCN pincer palladacycle, via a key biaryl benzyl bromide intermediate **5** (Scheme 2) [13]. By changing the sulfur nucleophile in step c (Scheme 2), the ability to synthesize a library of SCN pincer ligands is possible. This provides the opportunity to vary the thioether substituent to tune the steric and electronic properties of the sulfur atom, which will be bound to the palladium atom in the resulting palladacycle. The SCN ligands then undergo C–H bond activation with in situ-generated $Pd(MeCN)_4(BF_4)$ [13,34] synthesizing a library of SCN pincer palladacycles **1b–1f** (Scheme 2, Table 1).

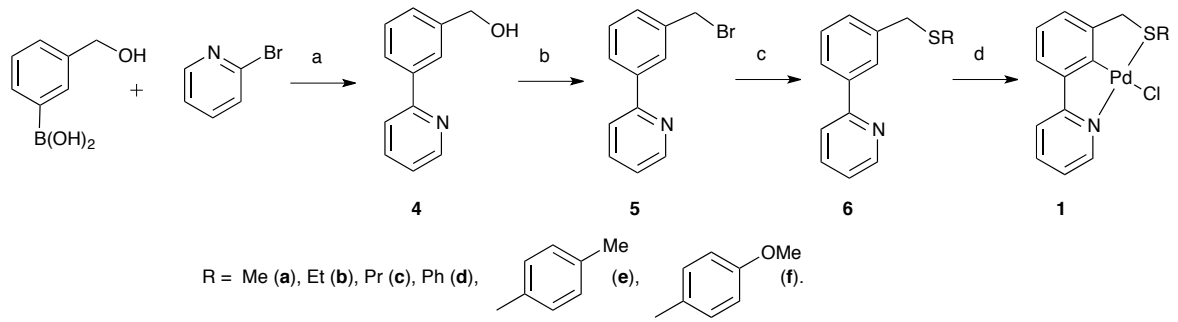

Scheme 2. A synthesis of SCN pincer palladacycles **1b–1f** via a key biaryl benzyl bromide intermediate **5**, based on the previous synthesis of **1a**. (Step a = $Pd(PPh_3)_4$, K_3PO_4, Tol/EtOH/H_2O; b = 48% HBr in H_2O; c = NaSMe, EtOH; d = (i) $PdCl_2$, $AgBF_4$, MeCN; and (ii) NaCl, H_2O/MeCN).

Table 1. SCN pincer palladacycle synthesis yields.

Entry	Palladacycle	Ligand Synthesis Conditions	Ligand Synthesis Isolated Yield/%	Palladacycle Synthesis Yield/%
1	**1b**	A	72	83
2	**1c**	B	>99	85
3	**1d**	B	99	71
4	**1e**	C	51	89
5	**1f**	B	60	54

A = NaH, DMF, MW 150 °C 15 min, B = NaH, DMF, MW 150 °C 20 min, C = NEt_3, EtOH, MW 150 °C 20 min.

The SCN ligand syntheses presented in Table 1 reveal excellent to moderate yields, followed by C–H bond activation, also in moderate to excellent yield. Single crystals of palladacycles **1b–d** and **1f** were obtained by slow evaporation of dichloromethane (DCM) from a saturated solution, and were characterized by X-ray crystallography (Figure 2). The CCDC numbers for the structures

are 1486787 for **1b**, 1486788 for **1c**, 1486789 for **1d** and 1486790 for **1f**. The data can be obtained free of charge from The Cambridge Crystallographic Data Centre via www.ccdc.cam.ac.uk/structures.

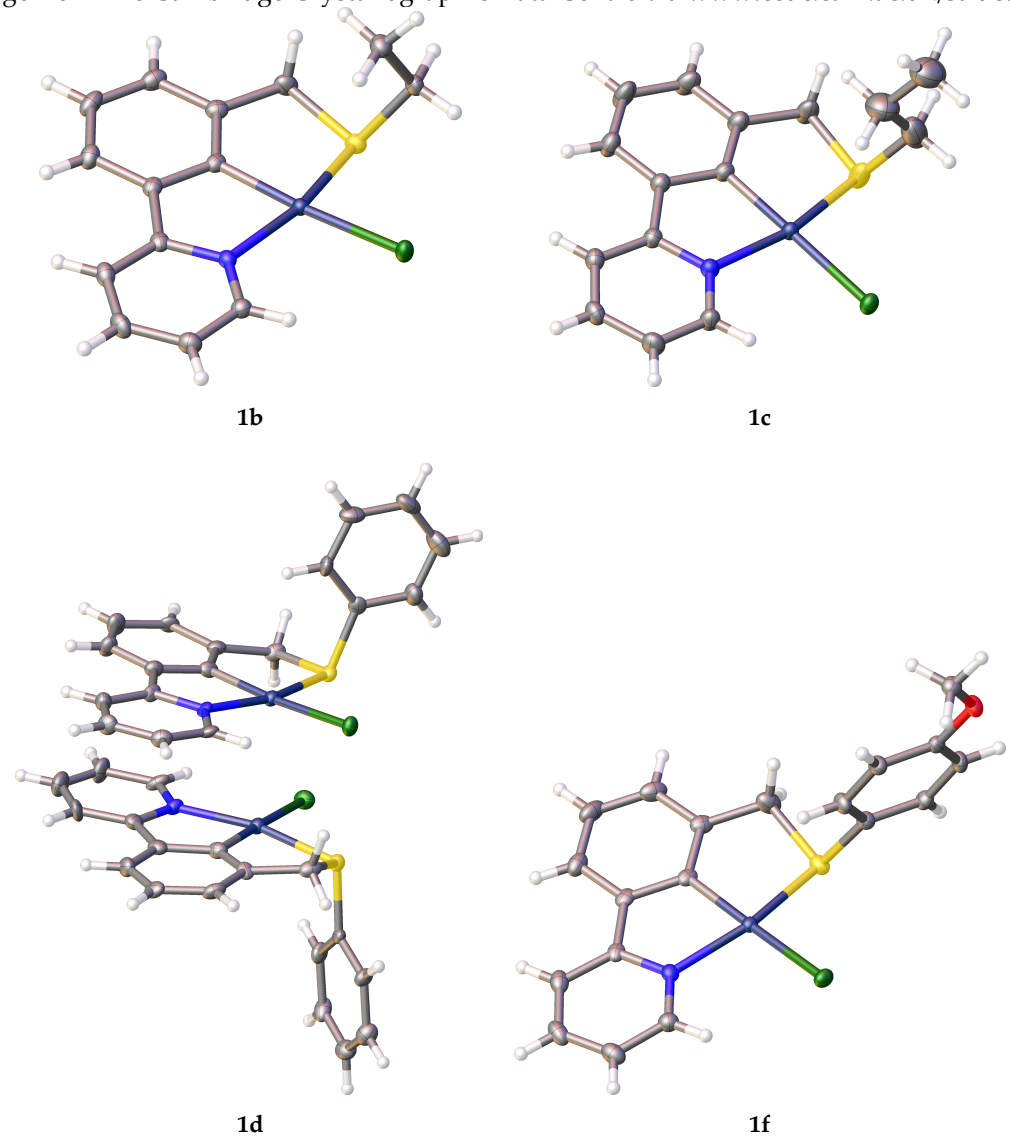

Figure 2. X-ray crystallographic structures of **1b–d**, **1f**.

2.2. Investigaing the Trans Influence

To determine the accuracy of the Perdew–Burke–Ernzerhof exchange–correlation functional (PBE) for optimizing the YCY′ pincer complexes, we have analyzed the mean signed errors (MSE), which is the average of the deviation between calculation and experiment, and the mean unsigned errors (MUE), which is the average of the absolute deviation between calculated and experimental Pd–L bond lengths (L = Y, Y′, C and Cl). The MSE for **1a–1d**, **1f** is 0.001 Å, for **2a–2b** is 0.012 Å and for **3a–3c** is 0.001 Å. The MUE for **1a–1d**, **1f** is 0.017 Å, for **2a–2b** is 0.012 Å and for **3a–3c** is 0.001 Å.

A topological analysis of the electron density was performed using QTAIM. The bond path is a single line of locally-maximum density linking the nuclei of any two bonded atoms in a molecule [36]. The minimum along this path is defined as the bond critical point (BCP) and the magnitude of the electron density $\rho(\mathbf{r})$ at this point can be used to determine the strength of the interaction.

Several AIM parameters determined at the Pd–Y and Pd–Y′ BCPs are provided in the Supplementary Information (electron density $\rho(\mathbf{r})$, Laplacian of the density $\nabla^2\rho(\mathbf{r})$, delocalization index, ellipticity, bond degree parameter, etc.) which can be used to determine the nature and strength of the interaction; the conclusions regarding the nature of the bonding are in complete

agreement with our previous work on the nature of the bonding in symmetrical pincer palladacycles and, so, are not presented again here [35]. In the present work, the focus is on the *trans* influence and, so, the magnitude of the electron density $\rho(\mathbf{r})$ at the BCP is used to determine the increase or decrease in the strength of the Pd–Y interaction when the ligand *trans* to it is varied.

2.2.1. *Trans* Influence in Model Palladacycles **I–III**

Normally, the *trans* influence has been studied in systems with four monodentate ligands coordinated to the metal center to form a square planar complex. Furthermore, a *trans* Pt–Cl bond length, situated *trans* to the donor atom arm, of a square planar complex is normally used to consider the *trans* influence [37–40]. From the unsymmetrical SCN pincer palladacycle structures, we do not have a Cl atom for monitoring the strength of the *trans* influence in this way. Therefore, first, simple model palladacycles **I–III** (Figure 3) have been studied using DFT to evaluate the *trans* influence in CY palladacycles before studying the unsymmetrical YCY′ pincer palladacycles. The models **I–III** contain a Cl ligand *trans* to a donor atom group (NMe_2, SMe_2, and PMe_2, respectively) to monitor the strength of the *trans* influence. A topological analysis of the electron density was performed using QTAIM and the magnitude of the electron density $\rho(\mathbf{r})$ at the bond critical point (BCP), the minimum along the bond path between interacting atoms, was used to determine the strength of the Pd–Cl interaction. A larger $\rho(\mathbf{r})$ value corresponds to a stronger interaction between atoms [41] and, therefore, can be used to study the *trans* influence in palladacycles **I–III**. When $\rho(\mathbf{r})$ at the BCP of Pd–Cl bond has a high value (strong interaction), it indicates that the donor atom *trans* to Cl has a weak *trans* influence, whereas a low $\rho(\mathbf{r})$ value (weak interaction) indicates that the donor atom *trans* to the Pd–Cl bond has a strong *trans* influence. A relative change in bond length is a physical manifestation that indicates the strength of the *trans* influence. When the Pd–Cl bond is situated *trans* to a donor atom that exhibits a strong *trans* influence, the Pd–Cl bond lengthens compared to when the Pd–Cl bond is situated *trans* to a weak *trans* influence donor atom. The data provided in Table 2 show that the $\rho(\mathbf{r})$ value of the Pd–Cl bond of **III** is smaller than that in **II**, which is smaller than in **I**, indicating that the *trans* influence of PMe_2 is greater than that of SMe which is greater than NMe_2. The $\rho(\mathbf{r})$ data is supported by the bond lengths, with **I** having the shortest Pd–Cl bond length and **III** a significantly longer Pd–Cl bond length than in **I** and **II**, again demonstrating the stronger PMe_2 *trans* influence. Based on this analysis the ordering of the *trans* influence series is PMe_2 > SMe > NMe_2.

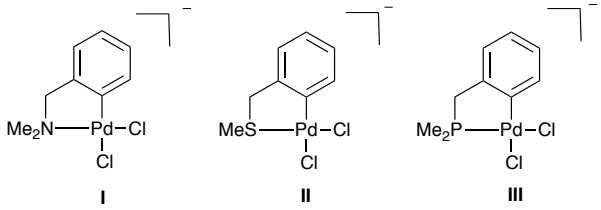

Figure 3. Model palladacycles **I–III** studied to investigate the *trans* influence.

Table 2. The electron density $\rho(\mathbf{r})$ and Pd–Cl bond lengths.

Compound	$\rho(\mathbf{r})$ of Pd–Cl (a.u.)	Pd–Cl Bond Length (Å)
I	0.080	2.334
II	0.077	2.352
III	0.070	2.395

2.2.2. *Trans* Influence in Model Unsymmetrical YCY′ Pincer Palladacycles

In order to extend our investigation of the *trans* influence to unsymmetrical pincer palladacycles, the palladacycles **IV**–**VI** have been studied using DFT and QTAIM, and their bond strengths and bond lengths compared to previous results found for symmetrical pincer palladacycles **PdNCN**, **PdSCS** and **PdPCP** [35] (Figure 4). Considering the $\rho(\mathbf{r})$ value at the BCP of the Pd–Y bond in **IV**–**VI**, the $\rho(\mathbf{r})$ value of the Pd–P bond of **V** (0.110 a.u) and **VI** (0.114 a.u.) are greater compared to the $\rho(\mathbf{r})$ values for the Pd–P bond in the **PdPCP** (0.101 a.u.) [35]. This is due to the weaker *trans* influence of N and S, compared to P, leading to stronger Pd–P bonds in **V** and **VI** (Table 3). The $\rho(\mathbf{r})$ value of the Pd–S bond of **IV** (0.097 a.u.) increases, whereas the $\rho(\mathbf{r})$ value of the Pd–S bond of **V** (0.082 a.u.) decreases, compared to the $\rho(\mathbf{r})$ value of the Pd–S bond in the **PdSCS** (0.091 a.u.), therefore showing that S has a moderate *trans* influence. Furthermore, the $\rho(\mathbf{r})$ values of the Pd–N bond of **IV** (0.083 a.u.) and **VI** (0.075 a.u.) decrease compared to the $\rho(\mathbf{r})$ value of the Pd–N bond in the **PdNCN** (0.086 a.u.) [35] indicating that P and S exhibit a stronger *trans* influence than N.

Supporting the $\rho(\mathbf{r})$ value results, the bond lengths of Pd–Y and Pd–Y′ are reported in Table 4. When the donor ligand Y has a *trans* influence the Pd–Y′ bond distance increases (and the $\rho(\mathbf{r})$ value decreases) indicating a weakened interaction. By comparing with the symmetrical YCY pincer palladacycles it can be seen that the P donor ligand has a *trans* influence on the S donor ligand and the N donor ligand, and that the S donor ligand has a *trans* influence on the N donor ligand. For example, in **VI**, the PCN palladacycle, the P donor ligand has a strong influence on the N donor ligand trans to it, which manifests as an increased Pd–N (2.203 Å) bond distance compared to the Pd–N bond in **PdNCN** (2.140 Å), and a commensurate decrease in the Pd–P bond distance (2.222 Å) compared to the Pd–P bond length in **PdPCP** (2.287 Å) (Table 4). The results confirm the conclusion from the model systems with Cl as a reference, that P exhibits the greatest *trans* influence and N the least.

Based on the $\rho(\mathbf{r})$ values and Pd–Y bond lengths, the ordering of the *trans* influence series is PMe_2 > SMe > NMe_2. This is in good agreement with that of Kapoor and Kakkar's study [40] into the square planar Pt complexes using DFT calculations. Their results showed a *trans* influence series in order of P > S > N. Moreover, Sajith and Suresh [42] studied the correlation between $\rho(\mathbf{r})$ and *trans* influence in a square planar Pd complex, showing good linear relation between $\rho(\mathbf{r})$ and *trans* influence, with a *trans* influence series of PMe_3 > SMe_2 > NH_3.

2.2.3. *Trans* Influence in Experimentally-Characterized Unsymmetrical YCY′ Pincer Palladacycles

In this section DFT and the QTAIM method is used to study the *trans* influence in **1a** (PdSCN), **2a** (PdPCN), and **3a** (PdN′CN). By comparing the Pd–N bond length in the structures **1a**, **2a**, and **3a** (optimized and experimental), the Pd–N bond is longest in **2a** and shortest in **3a** (Table 4). In addition, the smallest $\rho(\mathbf{r})$ values for the Pd–N bond is in **2a** (0.087 a.u.), while the largest is found in **3a** (0.102 a.u.) with **1a** (0.098 a.u.) intermediate (Table 3). The different Pd–N bond lengths and strengths demonstrate the difference in *trans* influence due to the nature of the donor atom of the Pd–Y bond. These results further confirm that the P donor ligand exhibits the strongest *trans* influence, while the N donor ligand has the weakest *trans* influence and that the *trans* influence series for the unsymmetrical pincer palladacycles considered is P > S > N.

The N donor ligand in the experimentally-characterized unsymmetrical SCN pincer palladacycle (Figure 1) is a pyridine rather than the amine considered in the previous section (**IV**). The change in electronic and steric effects when replacing NMe_2 (**IV**) with pyridine (**1a**) in a SCN pincer palladacyle is reflected in the bond strength: $\rho(\mathbf{r})$ value of the Pd–NMe_2 bond is 0.083 a.u. in **IV** whereas the Pd–pyr is 0.098 a.u. in **1a**, and the Pd–NMe_2 bond length is 2.156 Å in **IV** and the Pd–pyr bond length is 2.074 Å in **1a**, demonstrating the stronger Pd–pyridine bond (Tables 3 and 4). However, this does not appear to effect the *trans* influence exerted on the SMe ligand when *trans* to these N donor ligands. The $\rho(\mathbf{r})$ value of the Pd–S bond is 0.091 a.u. in **PdSCS** and increases to 0.097 a.u. in **IV** and 0.096 a.u. in **1a**, and the bond length in **PdSCS** is 2.313 Å and shortens to 2.285 Å in **IV** and 2.288 Å in **1a**. Thus, in both **IV** and **1a** the Pd–S bond is strengthened relative to the

symmetric **PdSCS** analog and, thus, can only be attributed to the effect of the N-donor ligand *trans* to it.

Furthermore, by comparing **PdNCN** where N = NMe_2, to PdNCN′ (**3a**), where one of the amine ligands has been replaced by pyridine, we can assess the *trans* influence in an unsymmetrical pincer palladacycle where the donor atom is the same (N) for distinctly different donor ligands (NMe_2 and pyr). In **3a** the ρ(**r**) value of the Pd–NMe_2 bond has not changed and the bond length has increased insignificantly (0.005 Å) from that in the symmetric **PdNCN** palladacycle. Therefore, we can conclude that, although the electronic and steric effects of the pyridine result in a considerably stronger bond to the Pd center, this stronger bond does not exert a *trans* influence on the amine donor ligand. Thus, it would appear the nature of the donor atom is the sole driver for the *trans* influence.

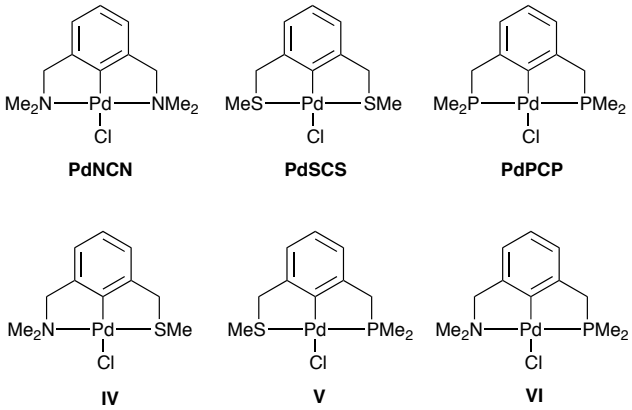

Figure 4. Symmetrical NCN, SCS, and PCP pincer palladacycles (**PdNCN**, **PdSCS** and **PdPCP**) [35] and model unsymmetrical SCN (**IV**), PCS (**V**), and PCN (**VI**) pincer palladacycles.

Table 3. Electron density ρ(**r**) in symmetrical and unsymmetrical pincer palladacycles (values are in atomic units). The donor atom is shown in bold for each side arm, Y and Y′.

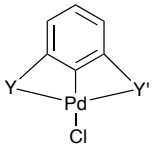

PdYCY′	Y	Y′	ρ(r) of Pd–Y	ρ(r) of Pd–Y′
PdNCN	Me_2**N**CH_2	Me_2**N**CH_2	0.086	0.086
PdSCS	Me**S**CH_2	Me**S**CH_2	0.091	0.091
PdPCP	Me_2**P**CH_2	Me_2**P**CH_2	0.101	0.101
IV	Me**S**CH_2	Me_2**N**CH_2	0.097	0.083
V	Me_2**P**CH_2	Me**S**CH_2	0.110	0.082
VI	Me_2**P**CH_2	Me_2**N**CH_2	0.114	0.075
1a	Me**S**CH_2	2-**N**C_5H_4	0.096	0.098
1b	Et**S**CH_2	2-**N**C_5H_4	0.095	0.098
1c	Pr**S**CH_2	2-**N**C_5H_4	0.095	0.098
1d	Ph**S**CH_2	2-**N**C_5H_4	0.092	0.098
1e	(*p*-MeC_6H_4)**S**CH_2	2-**N**C_5H_4	0.092	0.098
1f	(*p*-MeOC_6H_4)**S**CH_2	2-**N**C_5H_4	0.092	0.098
2a	Ph_2**P**O	2-**N**C_5H_4	0.114	0.087
2b	Ph_2**P**OCH_2	2-**N**C_5H_4	0.113	0.089
3a	Me_2**N**CH_2	2-**N**C_5H_4	0.086	0.102
3b	Et_2**N**CH_2	2-**N**C_5H_4	0.085	0.102
3c	(C_4H_8O)**N**CH_2	2-**N**C_5H_4	0.084	0.102

Table 4. Calculated and experimental Pd–Y and Pd–Y′ bond distances in symmetrical and unsymmetrical pincer palladacycles (bond distances are in Å). The donor atom is shown in bold for each side arm, Y and Y′.

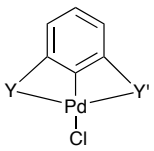

PdYCY′	Y	Y′	Calculation		X-ray		Ref. X-ray
			Pd–Y	Pd–Y′	Pd–Y	Pd–Y′	
PdNCN	Me$_2$**N**CH$_2$	Me$_2$**N**CH$_2$	2.140	2.140	2.103(3)	2.102(3)	[6]
PdSCS	Me**S**CH$_2$	Me**S**CH$_2$	2.313	2.313	2.2831(11)	2.2911(11)	[7]
PdPCP	Me$_2$**P**CH$_2$	Me$_2$**P**CH$_2$	2.287	2.287	n/a	n/a	n/a
IV	Me**S**CH$_2$	Me$_2$**N**CH$_2$	2.285	2.156	n/a	n/a	n/a
V	Me$_2$**P**CH$_2$	Me**S**CH$_2$	2.240	2.364	n/a	n/a	n/a
VI	Me$_2$**P**CH$_2$	Me$_2$**N**CH$_2$	2.222	2.203	n/a	n/a	n/a
1a	Me**S**CH$_2$	2-**N**C$_5$H$_4$	2.288	2.074	2.291(8)	2.09(3)	[13]
1b	Et**S**CH$_2$	2-**N**C$_5$H$_4$	2.290	2.076	2.2638(4)	2.0672(13)	*
1c	Pr**S**CH$_2$	2-**N**C$_5$H$_4$	2.291	2.076	2.2705(7)	2.066(2)	*
1d	Ph**S**CH$_2$	2-**N**C$_5$H$_4$	2.303	2.078	2.2846(17)	2.069(5)	*
1e	(*p*-MeC$_6$H$_4$)**S**CH$_2$	2-**N**C$_5$H$_4$	2.302	2.078	n/a	n/a	n/a
1f	(*p*-MeOC$_6$H$_4$)**S**CH$_2$	2-**N**C$_5$H$_4$	2.303	2.078	2.2674(5)	2.0708(15)	*
2a	Ph$_2$**P**O	2-**N**C$_5$H$_4$	2.219	2.129	2.2028(6)	2.1216(18)	[14]
2b	Ph$_2$**P**OCH$_2$	2-**N**C$_5$H$_4$	2.232	2.114	2.2159(7)	2.103(2)	[14]
3a	Me$_2$**N**CH$_2$	2-**N**C$_5$H$_4$	2.145	2.060	2.105(6)	2.062(5)	[14]
3b	Et$_2$**N**CH$_2$	2-**N**C$_5$H$_4$	2.149	2.063	2.1145(16)	2.0639(16)	[14]
3c	(C$_4$H$_8$O)**N**CH$_2$	2-**N**C$_5$H$_4$	2.154	2.060	2.1239(19)	2.0521(19)	[14]

* The result from this work. n/a: not available

2.2.4. *Trans* Influence on Unsymmetrical Pincer Palladacycles: Donor Atom Substituent Effects

To determine whether the *trans* influence is induced when the substituents on the donor atom are varied, thereby introducing subtle electronic effects, the library of SCN pincer palladacycles synthesized in the present work (**1b**-**1f**), along with **1a**, have been investigated computationally to determine the influence of the thioether group on the coordinated pyridine *trans* to it. The Pd–N bond distances (experimental and calculated) show very little change when the substituent on the S atom is changed (bond distance differences < 0.005 Å, with the exception of the experimental Pd–N bond length for **1a**) (Table 4). Similarly, the ρ(**r**) values at the Pd–N BCP in the SCN pincer palladacycles are unaffected by changing substitution on donor atom.

Furthermore, when the substituent is changed on the P (**2a** and **2b**) (which both incorporate the phosphinite donor group) or the N (**3a–3c**), Figure 1, it does not alter the *trans* influence on the Pd–pyr interaction within the PCN or N′CN pincer palladacycles. The ρ(**r**) values for the Pd–pyr bond *trans* to the Pd–N′ bond is independent of the nature of the N′ ligand, and although the interactions (ρ(**r**) and bond length) due to the Pd–P ligands exhibit a slight difference (0.002 a.u. and 0.015 Å) they are extremely small.

3. Experimental Section

3.1. General Details

Solvents and chemicals were purchased from Sigma-Aldrich (Merck KGaA, Damstadt, Germany), VWR International (VWR, Radnor, PA, USA), Fisher Scientific (Fisher Scientific UK Ltd., Loughborough, UK) and Fluorochem (Fluorochem Ltd., Hadfield, UK) and used without further purification, with reactions taking place open to atmosphere and moisture.

3.2. Instrumentation

^{1}H and ^{13}C spectra were recorded on either a Varian 400 or 500 MHz spectrometer (Agilent Technologies, Yarnton, UK). High resolution mass spectrometry (HRMS) data were obtained on an electrospray ionization (ESI) mass spectrometer using a Bruker Daltonics Apex III (Brucker, Billerica, MA, USA), with source Apollo ESI, using methanol as the spray. Flash chromatography was performed on an automated ISCO RF75 (Teledyne ISCO Inc., Licoln, NE, USA). Gas chromatography (GC) measurements were obtained using a Perkin Elmer Autosystem XL Gas Chromatograph (PerkinElmer Inc., Waltham, MA, USA), utilizing a flame ionization detector, and a Supelco MDN-5S 30 m × 0.25 mm × 0.25 μm column, with a He mobile phase. Elemental analyses were run by the London Metropolitan University Elemental Analysis Service (ThermoFisher Scientific, Waltham, MA, USA). Crystal structures were obtained by the UK National Crystallography Service at the University of Southampton [43].

3.3. Procedure

2-3-[(Ethylsulfanyl)methyl]phenylpyridine, **6b**. Under an argon atmosphere, ethanethiol (2.42 mmol, 0.179 mL) and sodium hydride (2.41 mmol, 58 mg) were dissolved in dry DMF (dimethylformamide, 3 mL) and stirred at room temperature in a sealed microwave vial for 15 min. 2-[3-(Bromomethyl)phenyl]pyridine, **5** (1.61 mmol, 400 mg) in dry DMF (3 mL) was then added, and stirred under microwave irradiation (maximum power 300 W, dynamic heating) at 150 °C for 15 min. After cooling, the solvent was removed in vacuo and the crude mixture was diluted in H_2O (25 mL) and DCM (25 mL). The product was extracted with DCM (2 × 25 mL), washed with H_2O (5 × 25 mL) and brine (25 mL). The organic layers were dried over anhydrous $MgSO_4$, filtered, and concentration in vacuo. The crude product was purified using flash column chromatography (7:3 DCM:EtOAc) yielding 263 mg of the expected product, **6c**, as a yellow oil in 71% yield. ^{1}H NMR (500 MHz), Chloroform-*d* δ (ppm): 8.70 (d, *J* = 4.8 Hz, 1H), 7.96 (s, 1H), 7.86 (d, *J* = 7.5 Hz, 1H), 7.77–7.73 (m, 2H), 7.43 (dd, *J* = 7.5, 7.5 Hz, 1H), 7.39 (d, *J* = 7.5 Hz, 1H), 7.24 (ddd, 6.3, 4.8, 2.3 Hz, 1H), 3.81 (s, 2H), 2.48 (q, *J* = 7.5 Hz, 2H), 1.25 (t, *J* = 7.5 Hz, 3H). ^{13}C NMR (126 MHz), Chloroform-*d* δ (ppm): 157.3, 149.7, 139.6, 139.2, 136.7, 129.4, 128.9, 127.4, 125.5, 122.1, 120.6, 36.0, 25.4, 14.4. HRMS (*m*/*z*). Calc. for $[C_{14}H_{15}NS + H]^+$ 230.0998. Found 230.0998.

2-3-[(Propylsulfanyl)methyl]phenylpyridine, **6c**. Same methodology as **6b**, using propane-1-thiol (1.97 mmol, 0.178 mL), and reacting for 20 min in the microwave. After workup, 300 mg of the expected product, **6c** was found, without purification in >99% yield as a yellow oil. ^{1}H NMR (500 MHz), Chloroform-*d* δ (ppm): 8.70 (d, *J* = 4.8 Hz, 1H), 7.96 (s, 1H), 7.86 (d, *J* = 7.5 Hz, 1H), 7.78–7.73 (m, 2H), 7.43 (dd, *J* = 7.5, 7.5 Hz, 1H), 7.39 (d, *J* = 7.5 Hz, 1H), 7.24 (ddd, *J* = 6.5, 4.8, 2.1 Hz, 1H), 3.79 (s, 2H), 2.44 (t, *J* = 7.2 Hz, 2H), 1.64–1.57 (m, 2H), 0.96 (t, *J* = 7.3 Hz, 3H).). ^{13}C NMR (126 MHz), Chloroform-*d* δ (ppm): 157.2, 149.6, 139.6, 139.3, 136.7, 129.4, 128.8, 127.4, 125.5, 122.1, 120.6, 36.3, 33.6, 22.6, 13.5. HRMS (*m*/*z*). Calc. for $[C_{15}H_{17}NS + H]^+$ 244.1154. Found 244.1155.

2-3-[(Phenylsulfanyl)methyl]phenylpyridine, **6d**. Same methodology as **6b**, using benzenethiol (1.86 mmol, 0.190 mL). After workup, 418 mg of the expected product, **6d** as a yellow oil in 99% yield. ^{1}H NMR (500 MHz), Chloroform-*d* δ (ppm): 8.70 (d, *J* = 4.8 Hz, 1H), 7.93 (s, 1H), 7.87 (d, *J* = 7.6 Hz, 1H), 7.76–7.72 (m, 2H), 7.67 (d, *J* = 8.0 Hz, 1H), 7.39 (dd, *J* = 7.6, 7.6 Hz, 1H), 7.36–7.33 (m, 2H), 7.27–7.21 (m, 3H), 7.20–7.16 (m, 1H), 4.20 (s, 2H). ^{13}C NMR (126 MHz), Chloroform-*d* δ (ppm): 157.2, 149.6, 139.6, 138.0, 136.7, 130.0 (2C), 129.3 (2C), 128.9, 128.8 (2C), 127.4, 126.4, 125.8, 122.1, 39.2.

2-(3-[(4-Methylphenyl)sulfanyl]methylphenyl)pyridine, **6e**. Under an argon atmosphere, 4-methylbenzenethiol (0.70 mmol, 87 mg) and trimethylamine (0.70 mmol, 0.099 mL) were dissolved in dry EtOH (2 mL) and stirred at room temperature in a sealed microwave vial for 15 min. 2-[3-(Bromomethyl)phenyl]pyridine, **5** (0.44 mmol, 110 mg) in dry EtOH (2 mL) was then added and the mixture was stirred under microwave irradiation (maximum power, 300 W, dynamic heating) at 150 °C for 20 min. After cooling, the solvent was removed in vacuo and the crude mixture diluted with H_2O (25 mL) and EtOAc (25 mL). The product was extracted with EtOAc (2 × 25 mL), washed with H_2O (2 × 25 mL) and brine (25 mL). The organic layers were dried over anhydrous $MgSO_4$, filtered and concentrated in vacuo. The crude product was purified by flash chromatography (8:2 hexane:Et_2O) yielding 65 mg of the expected product, **6e** as a yellow oil in 51% yield. ^{1}H NMR (500 MHz), Chloroform-*d* δ (ppm): 8.70 (d, *J* = 4.8 Hz, 1H), 7.90 (s, 1H), 7.87 (d, *J* = 7.6 Hz, 1H), 7.72 (m, 1H), 7.65 (d, *J* = 8.0 Hz, 1H), 7.39 (dd, *J* = 7.6, 7.6 Hz, 1H), 7.32 (d, *J* = 7.6 Hz, 1H), 7.25 (d, *J* = 8.1 Hz, 2H), 7.21 (ddd, *J* = 7.4, 4.8, 1.2 Hz), 7.06 (d, *J* = 8.1 Hz, 2H), 4.15 (s, 2H), 2.30 (s, 3H). ^{13}C NMR (126 MHz), Chloroform-*d* δ (ppm): 157.2, 149.6, 139.6, 138.3, 136.6, 132.4, 131.5, 130.9 (2C), 129.6 (2C), 129.3, 128.8, 127.4, 125.7, 122.1, 120.5, 39.9, 21.0. HRMS (m/z). Calc. for $[C_{19}H_{17}NS + H]^+$ 292.1154. Found 292.1151.

2-(3-[(4-Methoxyphenyl)sulfanyl]methylphenyl)pyridine, **6f**. Same method as **6b**, using 4-methoxybenzenethiol (1.10 mmol, 0.136 mL). The crude product was purified using flash column chromatography (9:1 DCM:hexane) yielding 203 mg of the expected product, **6f** as a yellow oil in 60% yield. ^{1}H NMR (500 MHz), Chloroform-*d* δ (ppm): 8.69 (ddd, *J* = 4.8, 1.8, 0.9 Hz, 1H), 7.86 (d, *J* = 7.7 Hz, 1H), 7.81 (s, 1H), 7.73 (ddd, *J* = 9.7, 7.9, 1.8 Hz, 1H), 7.65 (d, *J* = 7.7 Hz, 1H), 7.37 (dd, *J* = 7.7, 7.7 Hz, 1H), 7.28 (d, *J* = 8.8 Hz, 2H), 7.25–7.21 (m, 2H), 6.79 (d, *J* = 8.8 Hz, 2H), 4.07 (s, 2H), 3.76 (s, 3H). ^{13}C NMR (126 MHz), Chloroform-*d* δ (ppm): 159.3, 157.2, 149.6, 139.5, 138.6, 136.6, 134.2 (2C), 129.4, 128.8, 127.5, 126.0 (2C), 125.6, 122.1, 120.6, 114.5, 55.3, 41.3. HRMS (*m*/*z*). Calc. for $[C_{19}H_{17}NOS + H]^+$ 308.1104. Found 308.1109.

2-3-[(Ethylsulfanyl)methyl]phenylpyridine chloro-palladacycle, **1b**. Under an argon atmosphere, $PdCl_2$ (1.17 mmol, 208 mg) was dissolved in dry MeCN (10 mL) and heated under reflux until a red solution had formed. $AgBF_4$ (2.36 mmol, 460 mg) in dry MeCN (5 mL) was added to the $PdCl_2$ solution and heated under reflux for 2 h, forming a white precipitate. The precipitate was filtered off, and **6b** (1.13 mmol, 260 mg) dissolved in dry MeCN (10 mL), was added to the filtrate and heated under reflux for 4 h. The solution was cooled to room temperature, filtered over celite, and the solvent removed in vacuo. The crude solid was dissolved in MeCN (5 mL), and NaCl (26.0 mmol, 1.52 g) dissolved in H_2O (5 mL) was added, and stirred at room temperature for 3 h. The solvent was removed in vacuo, and the crude mixture dissolved in DCM (25 mL) and H_2O (25 mL). The crude product was extracted with DCM (2 × 25 mL), washed with H_2O (2 × 25 mL) and brine (25 mL), and dried over anhydrous Na_2SO_4. The mixture was filtered over celite, and the solvent removed in vacuo, yielding 347 mg of the expected product, **1b** as a yellow solid in 83% yield. ^{1}H NMR (500 MHz), Chloroform-*d* δ (ppm): 9.15 (d, *J* = 5.5 Hz, 1H), 7.84 (ddd, *J* = 7.8, 7.8 Hz, 1H), 7.64 (d, *J* = 7.8 Hz, 1H), 7.33 (d, *J* = 7.7 Hz, 1H), 7.26–7.23 (m, 1H), 7.08 (dd, *J* = 7.7, 7.7 Hz, 1H), 7.03 (d, *J* = 7.7 Hz, 1H), 4.25 (bs, 2H), 3.20 (q, *J* = 7.4 Hz, 2H), 1.57 (t, *J* = 7.4 Hz, 3H). ^{13}C NMR (126 MHz), Chloroform-*d* δ (ppm): 165.5, 165.3, 150.5, 148.1, 144.4, 139.0, 125.0, 124.7, 122.9, 122.2, 118.7, 45.8, 33.8, 14.8. HRMS (*m*/*z*). Calc. for $[C_{14}H_{14}NPdS]^+$ 333.9876. Found 333.9878. Elemental Analysis. Calc. (%) for $C_{14}H_{14}NPdSCl$: C 45.42, H 3.81, N 3.78; found C 45.50, H 3.75, N 3.83.

2-3-[(Propylsulfanyl)methyl]phenylpyridine chloro-palladacycle, **1c**. Same method as **1b** using **6c** (0.55 mmol, 113 mg), yielding 179 mg of the expected product, **1c** as a yellow solid in 85% yield. ^{1}H NMR (500 MHz), Chloroform-*d* δ (ppm): 9.11 (d, *J* = 5.5 Hz, 1H), 7.82 (ddd, *J* = 7.8, 7.8, 1.7 Hz, 1H), 7.62 (d, *J* = 7.7 Hz, 1H), 7.30 (d, *J* = 7.8 Hz, 1H), 7.22 (ddd, *J* = 7.5, 5.5, 1.3 Hz, 1H), 7.05 (dd, 7.7, 7.7 Hz, 1H), 7.00 (d, *J* = 7.7 Hz, 1H), 4.27 (bs, 2H), 3.15 (t, *J* = 7.8 Hz, 2H), 1.96 (m, 2H), 1.07 (t, *J* = 7.4 Hz, 3H). ^{13}C NMR (126 MHz), Chloroform-*d* δ (ppm): 165.5, 165.3, 150.5, 148.1, 144.4, 139.0, 125.0, 124.6, 122.9, 122.1, 118.7, 46.6, 41.4, 23.3, 13.3. HRMS (*m*/*z*). Calc. for $[C_{15}H_{16}NPdS]^+$ 348.0033. Found

348.0032. Elemental Analysis. Calc. (%) for $C_{15}H_{16}NPdSCl$: C 46.89, H 4.20, N 3.65; found: C 47.02, H 4.08, N 3.56.

2-3-[(Phenylsulfanyl)methyl]phenylpyridine chloro-palladacycle, **1d**. Same method as **1b** using **6d** (1.51 mmol, 418 mg). The crude product was purified using flash column chromatography (100% consisting of 98:2 DCM:MeOH) yielding 446 mg of the expected product **1d** as a yellow solid in 71% yield. ^{1}H NMR (500 MHz), Chloroform-*d* δ (ppm): 9.14 (d, *J* = 5.5 Hz, 1H), 7.91–7.89 (m, 2H), 7.83 (ddd, *J* = 7.7, 7.7, 1.7 Hz, 1H), 7.62 (d, *J* = 7.7 Hz, 1H), 7.36–7.33 (m, 3H), 7.29 (d, *J* = 7.7 Hz, 1H), 7.20 (ddd, *J* = 7.7, 5.5, 1.2 Hz, 1H), 7.06 (dd, *J* = 7.7, 7.7 Hz, 1H), 7.00 (d, *J* = 7.7 Hz, 1H), 4.63 (s, 2H). ^{13}C NMR (126 MHz), Chloroform-*d* δ (ppm): 166.0, 165.5, 150.8, 147.8, 144.6, 139.1, 132.8, 131.9 (2C), 129.9, 129.6 (2C), 124.9, 124.8, 122.9, 122.3, 118.8, 53.1. HRMS (*m*/*z*). Calc. for $[C_{18}H_{14}NPdS]^{+}$ 381.9876. Found 381.9876. Elemental Analysis. Calc. (%) for $C_{18}H_{14}NPdSCl$: C 51.69, H 3.37, N 3.35; found C 51.50, H 3.28, N 3.41.

2-(3-[(4-Methylphenyl)sulfanyl]methylphenyl)pyridine, **1e**. Same method as **1b**, using **6e** (0.54 mmol, 158 mg). ^{1}H NMR (500 MHz), Chloroform-*d* δ (ppm): 9.19 (d, *J* = 5.5 Hz, 1H), 7.84 (dd, *J* = 7.6, 7.6 Hz, 1H), 7.79 (d, *J* = 8.1 Hz, 2H), 7.64 (d, *J* = 7.6 Hz, 1H), 7.33 (d, *J* = 7.6 Hz, 1H), 7.23–7.21 (m, 1H), 7.16 (d, *J* = 8.1 Hz, 2H), 7.08 (dd, *J* = 7.6, 7.6 Hz, 1H), 7.00 (d, *J* = 7.6 z, 1H), 4.60 (bs, 2H), 2.32 (s, 3H). ^{13}C NMR (126 MHz), Chloroform-*d* δ (ppm): 166.0, 165.5, 150.7, 147.9, 144.5, 140.4, 139.1, 132.0 (2C), 130.3 (2C), 129.4, 124.8, 122.9, 122.2, 118.8, 53.5, 21.2. HRMS (*m*/*z*). Calc. for $[C_{19}H_{16}NPdS]^{+}$ 396.0033. Found 396.0050. Elemental Analysis. Calc. (%) for $C_{19}H_{16}NPdSCl$: C 52.63, H 3.84, N 3.29; found C 52.79, H 3.73, N 3.24.

2-(3-[(4-Methoxyphenyl)sulfanyl]methylphenyl)pyridine, **1f**. Same method as **1b**, using **1e** (0.62 mmol, 190 mg). ^{1}H NMR (500 MHz), Chloroform-*d* δ (ppm): 9.18 (d, *J* = 5.5 Hz, 1H), 7.86–7.83 (m, 3H), 7.65 (d, *J* = 7.9 Hz, 1H), 7.33 (d, *J* = 7.6 Hz, 1H), 7.23 (ddd, *J* = 7.6, 5.5, 1.4 Hz, 1H), 7.08 (dd, *J* = 7.6, 7.6 Hz, 1H), 6.99 (d, *J* = 7.6 Hz, 1H), 6.87 (d, *J* = 8.9 Hz, 1H), 4.58 (s, 2H), 3.77 (s, 3H). ^{13}C NMR (126 MHz), Chloroform-*d* δ (ppm): 165.9, 165.5, 161.2, 150.8, 147.8, 144.5, 139.1, 134.0 (2C), 124.8, 123.5, 122.9, 122.2, 118.8, 115.1 (2C), 55.5, 54.4. HRMS (m/z). Calc. for $[C_{19}H_{16}NOPdS]^{+}$ 411.9982. Found 411.9991. Elemental Analysis. Calc. (%) for $C_{19}H_{16}NOPdSCl$: C 50.91, H 3.60, N 3.12; found C 50.80, H 3.47, N 3.19.

4. Computational Section

Geometry optimization calculations were performed using Gaussian09 [44], in the gas-phase. The minimized structures were confirmed by the absence of any imaginary modes of vibration using frequency analysis. All structures were optimized using the generalized gradient approximation (GGA) PBE density functional [45,46]. The SDD ECP basis set was used for Pd, and the 6-31+G(d,p) basis set was used for all other atoms (PBE/6-31+G(d,p)[SDD]). This methodology has been validated in our previous study into the structures of symmetrical pincer palladacycles [35]. The topological analysis using quantum theory of atoms in molecules (QTAIM) was performed using the Multiwfn program [47]. The ωB97XD[48]/6-311+G(2df,2p)[DGDZVP] model chemistry was used for these calculations. The all-electron relativistic DGDZVP basis set was used to treat Pd [49] as the bond path cannot be traced when treated using ECP.

5. Conclusions

It has been shown that the *trans* influence plays a key role in the stability of unsymmetrical pincer palladacycles, with the bond strength, and the bond length of the Pd-donor atom interaction affected significantly when *trans* to a ligand exhibiting a strong *trans* influence. The topological analysis of the electron density at the bond critical point, and the structure determination, show that the strength of the *trans* influence is in the order P > S > N. This is in agreement with previous work [40,42].

A library of SCN pincer palladacycles were synthesized via C–H bond activation and characterized using X-ray crystallography, demonstrating the utility of late stage derivitization.

These SCN palladacycles, along with PCN and N'CN previously synthesized by the authors, were used to investigate the driving force for the *trans* influence. It was shown, by investigating the electron density at the bond critical point and changes in the Pd-donor ligand bond length, that it is the donor atom that is responsible for the *trans* influence. The electronic and steric factors of the ligand do not influence significantly the bond strength of the ligand *trans* to it. This demonstrates the important role of unsymmetrical pincer palladacycles, with different donor atoms, in the search for harnessing and exploiting hemilability in the design of effective new palladacycle catalysts.

Supplementary Materials: The following are available online at www.mdpi.com/2304-6740/4/3/25/s1, Section S1: QTAIM key parameters (electron density $\rho(\mathbf{r})$, Laplacian of the electron density $\nabla^2\rho(\mathbf{r})$, total energy $H(\mathbf{r})$, bond degree parameter $|H(\mathbf{r})/\rho(\mathbf{r})|$, ellipticity ε, delocalization index δ, at the BCP of Pd–Cl (Table S1) and at the BCPs of Pd–Y and Pd–Y' (Table S2). Section S2: Cartesian coordinates and Section S3: Experimental spectral data.

Acknowledgments: We would like to thank the University of Sussex for a studentship (GWR), Royal Thai Government for scholarship (SB) and Christopher Dadswell for the support and use of the GC equipment, and Johnson Matthey for the loan of palladium salts. We would also like to thank Alaa Abdul-Sada at the University of Sussex and the EPSRC Mass Spectroscopy Service (University of Swansea) for mass spectrometry services.

Author Contributions: Sarote Boonseng performed the calculations, interpreted the data and wrote the theoretical section. Gavin W. Roffe performed the experiments, interpreted their data and wrote the experimental section. Rhiannon N. Jones synthesized **1d**. Simon J. Coles and Graham J. Tizzard performed X-ray crystal structure analysis. Hazel Cox and John Spencer provided the idea, supervised the project and revised the manuscript.

Conflicts of Interest: The authors declare no conflict of interest.

Abbreviations

Pyr: Pyridine
DFT: Density Functional Theory
QTAIM: Quantum Theory of Atoms in Molecules
Tol: Toluene
HRMS: High Resolution Mass Spectrometry
ESI: Electrospray Ionization
GC: Gas Chromatography
DMF: Dimethylformamide
DCM: Dichloromethane
PBE: Perdew Burke Ernzerhof Exchange–Correlation Functional
MSE: Mean Signed Error
MUE: Mean Unsigned Error
BCP: Bond Critical Point
GGA: Generalized Gradient Approximation
SDD: Stuttgart-Dresden
ECP: Effective Core Potentials

References

1. Cope, A.C.; Siekman, R.W. Formation of covalent bonds from platinum or palladium to carbon by direct substitution. *J. Am. Chem. Soc.* **1965**, *87*, 3272–3273.
2. Dupont, J.; Consorti, C.S.; Spencer, J. The potential of palladacycles: More than just precatalysts. *Chem. Rev.* **2005**, *105*, 2527–2571.
3. Niu, J.-L.; Hao, X.-Q.; Gong, J.-F.; Song, M.-P. Symmetrical and unsymmetrical pincer complexes with group 10 metals: Synthesis via aryl C–H activation and some catalytic applications. *Dalton Trans.* **2011**, *40*, 5135–5150.
4. Selander, N.; Szabó, K.J. Catalysis by palladium pincer complexes. *Chem. Rev.* **2011**, *111*, 2048–2076.
5. Morales-Morales, D. Pincer complexes. Applications in catalysis. *Rev. Soc. Quim. Mex*. **2004**, *48*, 338–346.

6. Liu, B.-B.; Wang, X.-R.; Guo, Z.-F.; Lu, Z.-L. Mononuclear versus dinuclear palladacycles derived from 1,3-bis(*N*,*N*-dimethylaminomethyl)benzene: Structures and catalytic activity. *Inorg. Chem. Commun.* **2010**, *13*, 814–817.
7. Kruithof, C.A.; Dijkstra, H.P.; Lutz, M.; Spek, A.L.; Gebbink, R.J.M.K.; van Koten, G. X-Ray and NMR study of the structural features of SCS-pincer metal complexes of the group 10 triad. *Organometallics* **2008**, *27*, 4928–4937.
8. Kjellgren, J.; Aydin, J.; Wallner, O.A.; Saltanova, I.V.; Szabó, K.J. Palladium pincer complex catalyzed cross-coupling of vinyl epoxides and aziridines with organoboronic acids. *Chem. Eur. J.* **2005**, *11*, 5260–5268.
9. Yao, Q.; Sheets, M. A SeCSe−Pd(II) pincer complex as a highly efficient catalyst for allylation of aldehydes with allyltributyltin. *J. Org. Chem.* **2006**, *71*, 5384–5387.
10. Aydin, J.; Selander, N.; Szabó, K.J. Strategies for fine-tuning the catalytic activity of pincer-complexes. *Tetrahedron Lett.* **2006**, *47*, 8999–9001.
11. Gagliardo, M.; Selander, N.; Mehendale, N.C.; Van Koten, G.; Klein Gebbink, R.J.M.; Szabó, K.J. Catalytic performance of symmetrical and unsymmetrical sulfur-containing pincer complexes: Synthesis and tandem catalytic activity of the first PCS-pincer palladium complex. *Chem. Eur. J.* **2008**, *14*, 4800–4809.
12. Moreno, I.; SanMartin, R.; Ines, B.; Herrero, M.T.; Domínguez, E. Recent advances in the use of unsymmetrical palladium pincer complexes. *Curr. Org. Chem.* **2009**, *13*, 878–895.
13. Roffe, G.W.; Boonseng, S.; Baltus, C.B.; Coles, S.J.; Day, I.J.; Jones, R.N.; Press, N.J.; Ruiz, M.; Tizzard, G.J.; Cox, H.; et al. A synthetic, catalytic and theoretical investigation of an unsymmetrical SCN pincer palladacycle. *R. Soc. Open Sci.* **2016**, *3*, doi:10.1098/rsos.150656.
14. Roffe, G.W.; Tizzard, G.J.; Coles, S.J.; Cox, H.; Spencer, J. Synthesis of unsymmetrical N'CN and PCN pincer palladacycles and their catalytic evaluation compared with a related SCN pincer palladacycle. *Org. Chem. Front.* **2016**, *3*, 957–965.
15. Braunstein, P.; Naud, F. Hemilability of hybrid ligands and the coordination chemistry of oxazoline-based systems. *Angew. Chem. Int. Ed.* **2001**, *40*, 680–699.
16. Khusnutdinova, J.R.; Milstein, D. Metal-ligand cooperation. *Angew. Chem. Int. Ed.* **2015**, *54*, 12236–12273.
17. Zhang, W.H.; Chien, S.W.; Hor, T.S.A. Recent advances in metal catalysts with hybrid ligands. *Coord. Chem. Rev.* **2011**, *255*, 1991–2024.
18. Ramírez-Rave, S.; Estudiante-Negrete, F.; Toscano, R.A.; Hernández-Ortega, S.; Morales-Morales, D.; Grévy, J.M. Synthesis and characterization of new Pd(II) non-symmetrical Pincer complexes derived from thioether functionalized iminophosphoranes. Evaluation of their catalytic activity in the Suzuki–Miyaura couplings. *J. Organomet. Chem.* **2014**, *749*, 287–295.
19. Saha, D.; Verma, R.; Kumar, D.; Pathak, S.; Bhunya, S.; Sarkar, A. A "hemilabile" palladium–carbon bond: Characterization and its implication in catalysis. *Organometallics* **2014**, *33*, 3243–3246.
20. Poverenov, E.; Gandelman, M.; Shimon, L.J.W.; Rozenberg, H.; Ben-David, Y.; Milstein, D. Pincer "hemilabile" effect. PCN platinum(II) complexes with different amine "arm length." *Organometallics* **2005**, *24*, 1082–1090.
21. Gargir, M.; Ben-David, Y.; Leitus, G.; Diskin-Posner, Y.; Shimon, L.J.W.; Milstein, D. PNS-Type ruthenium pincer complexes. *Organometallics* **2012**, *31*, 6207–6214.
22. Fleckhaus, A.; Mousa, A.H.; Lawal, N.S.; Kazemifar, N.K.; Wendt, O.F. Aromatic PCN palladium pincer complexes. Probing the hemilability through reactions with nucleophiles. *Organometallics* **2015**, *34*, 1627–1634.
23. Pidcock, A.; Richards, R.E.; Venanzi, L.M. ^{195}Pt–^{31}P nuclear spin coupling constants and the nature of the *trans*-effect in platinum complexes. *J. Chem. Soc. A Inorg. Phys. Theor.* **1966**, 1707–1710, doi:10.1039/j19660001707.
24. Appleton, T.G.; Clark, H.C.; Manzer, L.E. The trans-influence: Its measurement and significance. *Coord. Chem. Rev.* **1973**, *10*, 335–422.
25. Quagliano, J.V.; Schubert, L. The *trans* effect in complex inorganic compounds. *Chem. Rev.* **1952**, *50*, 201–260.
26. Rigamonti, L.; Rusconi, M.; Manassero, C.; Manassero, M.; Pasini, A. Quantification of *cis* and *trans* influences in $[PtX(PPh_3)_3]^+$ complexes. A ^{31}P NMR study. *Inorg. Chim. Acta* **2010**, *363*, 3498–3505.

27. Randaccio, L.; Bresciani-Pahor, N.; Toscano, P.J.; Marzilli, L.G. Bonding mode and *trans* influence of the nitromethyl ligand. Structure of *trans*-bis(dimethylglyoximato)(nitromethyl)(pyridine)cobalt(III). *Inorg. Chem.* **1981**, *20*, 2722–2724.
28. Otto, S.; Johansson, M.H. Quantifying the *trans* influence of triphenylarsine. Crystal and molecular structures of *cis*-[$PtCl_2(SMe_2)(AsPh_3)$] and *cis*-[$PtCl_2(AsPh_3)_2$]·$CHCl_3$. *Inorg. Chim. Acta* **2002**, *329*, 135–140.
29. Kaltsoyannis, N.; Mountford, P. Theoretical study of the geometric and electronic structures of pseudo-octahedral d^0 imido compounds of titanium: The *trans* influence in *mer*-[$Ti(NR)Cl_2(NH_3)_3$] (R = Bu^t, C_6H_5 or $C_6H_4NO_2$-4). *Dalt. Trans.* **1999**, 781–790, doi:10.1039/a807136e.
30. Lyne, P.D.; P. Mingos, D.M. The effects of back-bonding to phosphines on the *trans* influence in [$Mo(NH)Cl_3(PR_3)_2]^{0,\pm1}$ (R = H, Me and F). *J. Organomet. Chem.* **1994**, *478*, 141–151.
31. Jacobsen, H.; Berke, H. Tuning of the transition metal hydrogen bond: How do trans ligands influence bond strength and hydridicity? *Dalt. Trans.* **2002**, 3117–3122, doi:10.1039/b111085n.
32. Deeth, R.J. The trans influence in [$RH(Ph_3)_3Cl$]: A density functional theory study. *Dalt. Trans.* **1993**, 3711–3713, doi:10.1039/dt9930003711.
33. Burdett, J.K.; Albright, T.A. *Trans* influence and mutual influence of ligands coordinated to a central atom. *Inorg. Chem.* **1979**, *18*, 2112–2120.
34. Loeb, S.J.; Shimizu, G.K.H.; Wisner, J.A. Mono- versus dipalladation of the durene-based tetrathioether Ligand 1,2,4,5-(tBuSCH_2)$_4C_6H_2$. Structures of [$PdCl((t$BuS$CH_2)_4C_6H)$] and [$Pd_2((t$BuS$CH_2)_4C_6)(MeCN)_2][BF_4]_2$. *Organometallics* **1998**, *17*, 2324–2327.
35. Boonseng, S.; Roffe, G.W.; Spencer, J.; Cox, H. The nature of the bonding in symmetrical pincer palladacycles. *Dalt. Trans.* **2015**, *44*, 7570–7577.
36. Bader, R.F.W. A bond path: A universal indicator of bonded interactions. *J. Phys. Chem. A* **1998**, *5639*, 7314–7323.
37. Hartley, F.R. The *cis*- and *trans*-effects of ligands. *Chem. Soc. Rev.* **1973**, *2*, doi:10.1039/cs9730200163.
38. Sajith, P.K.; Suresh, C.H. Bond dissociation energies of ligands in square planar Pd(II) and Pt(II) complexes: An assessment using *trans* influence. *J. Organomet. Chem.* **2011**, *696*, 2086–2092.
39. Manojlovic-Muir, L.J.; Muir, K.W. The *trans*-influence of ligands in platinum(II) complexes. The significance of the bond length data. *Inorg. Chim. Acta* **1974**, *10*, 47–49.
40. Kapoor, P.N.; Kakkar, R. *Trans* and *cis* influence in square planar Pt(II) complexes: A density functional study of [$PtClX(dms)_2$] and related complexes. *J. Mol. Struct. Theochem*. **2004**, *679*, 149–156.
41. Bader, R.F.W. *Atoms in Molecules: A Quantum Theory*; Oxford University Press: Oxford, UK, 1990.
42. Sajith, P.K.; Suresh, C.H. Quantification of mutual trans influence of ligands in Pd(II) complexes: A combined approach using isodesmic reactions and AIM analysis. *Dalton Trans.* **2010**, *39*, 815–822.
43. Coles, S.J.; Gale, P.A. Changing and challenging times for service crystallography. *Chem. Sci.* **2012**, *3*, 683–689.
44. Frisch, M.J.; Trucks, G.W.; Schlegel, H.B.; Scuseria, G.E.; Robb, M.A.; Cheeseman, J.R.; Scalmani, G.; Barone, V.; Mennucci, B.; Petersson, G.A.; et al. Gaussian 09, Revision B.01. Gaussian, Inc.: Wallingford, CT, USA. **2009**.
45. Perdew, J.P.; Burke, K.; Ernzerhof, M. Generalized gradient approximation made simple. *Phys. Rev. Lett.* **1996**, *77*, 3865–3868.
46. Perdew, J.P.; Burke, K.; Ernzerhof, M. Generalized gradient approximation made simple [*Phys. Rev. Lett. 77*, 3865 (1996)]. *Phys. Rev. Lett.* **1997**, *78*, 1396.
47. Lu, T.; Chen, F. Multiwfn: A multifunctional wavefunction analyzer. *J. Comput. Chem.* **2012**, *33*, 580–592.
48. Chai, J.-D.; Head-Gordon, M. Long-Range corrected hybrid density functionals with damped atom–atom dispersion corrections. *Phys. Chem. Chem. Phys.* **2008**, *10*, 6615–6620.
49. Sajith, P.K.; Suresh, C.H. Mechanisms of reductive eliminations in square planar Pd(II) complexes: Nature of eliminated bonds and role of *trans* influence. *Inorg. Chem.* **2011**, *50*, 8085–8093.